Available online at www.sciencedirect.com

ScienceDirect

Ceramics International 39 (2013) 9163–9172

CERAMICS INTERNATIONAL

www.elsevier.com/locate/ceramint

Hydrothermal synthesis and visible-light photocatalytic activity of porous peanut-like $BiVO_4$ and $BiVO_4/Fe_3O_4$ submicron structures

Gangqiang Zhu[a,b,*], Mirabbos Hojamberdiev[c], Wenxiu Que[b], Peng Liu[a]

[a]School of Physics and Information Technology, Shaanxi Normal University, Xi'an 710062, PR China
[b]Electronic Materials Research Laboratory, School of Electronic and Information Engineering, Xi'an Jiaotong University, Xi'an 710049, PR China
[c]Materials and Structures Laboratory, Tokyo Institute of Technology, 4259 Nagatsuta, Midori, Yokohama, Kanagawa 226-8503, Japan

Received 25 March 2013; received in revised form 5 May 2013; accepted 5 May 2013
Available online 17 May 2013

Abstract

Porous peanut-like $BiVO_4$ and $BiVO_4/Fe_3O_4$ submicron structures were synthesized by a template-free hydrothermal process at 160 °C for 24 h. The as-synthesized samples were characterized by X-ray powder diffraction (XRD), scanning electron microscopy (SEM), transmission electron microscopy (TEM), X-ray photoelectron spectroscopy (XPS), vibrating sample magnetometer (VSM) and UV–vis spectroscopy. The photocatalytic activity of $BiVO_4$ and $BiVO_4/Fe_3O_4$ submicron structures were evaluated for the degradation of Rhodamine B (RhB) and methylene blue (MB) under visible light irradiation with and without the assistance of H_2O_2. According to the experimental results obtained, porous peanut-like $BiVO_4/Fe_3O_4$ composite photocatalyst shows higher photocatalytic activity in the H_2O_2-assisted system under visible light irradiation compared to $BiVO_4$. Recycling test on the $BiVO_4/Fe_3O_4$ composite photocatalyst for the degradation of RhB under visible light irradiation indicates that the composite photocatalyst is stable in the H_2O_2-assisted system in five cycles. Therefore, this composite photocatalyst will be beneficial for efficient degradation of organic pollutants present in water and air under solar light.

Keywords: Bismuth vanadate; Composite photocatalyst; Hydrothermal synthesis; Magnetite; Visible light irradiation

1. Introduction

Water pollution has become one of the challenging environmental issues. Particularly, wastewater generated from various chemical industries has high concentration of organic compounds that are extremely toxic, carcinogenic and stable in nature. Since the photoinduced decomposition of water on TiO_2 electrode was reported, the photodegradation of organic water pollutants over semiconductor-based photocatalysts has attracted extensive research interest in the past twenty years [1–3]. Photocatalysis characterized by the generation of •OH radicals and other oxidative radicals involving in photocatalytic reactions is considered to be one of the most promising technologies for water purification. In addition, TiO_2 shows good disinfecting activity against a broad spectrum of microorganisms [4]. However, its low quantum yield and absorbance of near UV region ($\lambda < 400$ nm) limit its practical application. Therefore, the development of new, highly efficient visible light-responsive photocatalysts is important from the viewpoint of using solar energy to degrade organic pollutants.

Bismuth vanadate ($BiVO_4$) is considered as an important semiconductor because of its application as gas sensors, solid-state electrolytes, and positive electrode materials for rechargeable lithium-ion batteries [5–8]. Recently, $BiVO_4$ has been intensively studied for the photocatalytic evolution of O_2 and photodegradation of organic pollutants under visible light irradiation [9–12]. $BiVO_4$ is a layer-structured compound with three polymorphs: monoclinic scheelite, tetragonal zircon, and tetragonal scheelite [13]. As it is known, that the photocatalytic property of a material strongly

*Corresponding author at: School of Physics and Information Technology, Shaanxi Normal University, Xi'an 710062, PR China.
Tel./fax: +86 29 81530750.
E-mail address: zgq2006@snnu.edu.cn (G. Zhu).

0272-8842/$ - see front matter © 2013 Elsevier Ltd and Techna Group S.r.l. All rights reserved.
http://dx.doi.org/10.1016/j.ceramint.2013.05.017

depends on the crystal and band structures [14]. $BiVO_4$ with monoclinic structure shows higher photocatalytic activity due to its relatively narrow band gap of 2.4 eV compared to $BiVO_4$ with tetragonal structure (3.1 eV) [15,16]. In addition to its crystal and band structures, the microstructure of $BiVO_4$ is also important factor for enhanced photocatalytic activity. Hence, monoclinic $BiVO_4$ with different morphologies, such as nanospheres, nanoplates, nanosheets, nanotubes, mesoporous and hierarchical nanostructures, was synthesized by a surfactant-assisted hydrothermal method [17–23]. These particular nano- and microstructures of $BiVO_4$ demonstrate higher photocatalytic activity because of their high surface areas and specific structures.

Magnetite (Fe_3O_4) has been widely used in different applications, such as electronic devices, magnetic storage, sorption and biomedicine [24–26]. Particularly, it has shown good photocatalytic activity for the degradation of organic compounds, and it can be easily separated by magnetic separation. Magnetic separation is a very convenient approach that allows separating and recycling magnetic particles/composites after photodegradation reactions. So far, a number of composite photocatalysts containing magnetite have been synthesized, such as TiO_2/Fe_3O_4, Fe_3O_4/C/CdS, Bi_2O_3/Fe_3O_4, WO_3/Fe_3O_4, Fe_3O_4@C@Cu_2O, etc. [27–31]. As mentioned above, these composite photocatalysts not only possess enhanced visible light photocatalytic activity, but also good recyclability.

We report on the synthesis of porous peanut-like $BiVO_4$ and $BiVO_4/Fe_3O_4$ submicron structures by hydrothermal method. The photocatalytic activity of $BiVO_4$ and $BiVO_4/Fe_3O_4$ submicron structures are evaluated for the degradation of Rhodamine B (RhB) and methylene blue (MB) under visible light irradiation with and without the assistance of H_2O_2.

2. Experimental

2.1. Synthesis of Fe_3O_4 nanoparticles

Fe_3O_4 nanoparticles were synthesized by a chemical precipitation method at room temperature. First, 200 mL of deionized water was poured into a bottom round flask and deoxygenated by bubbling N_2 gas for 30 min, and then 50 mL of NH_4Cl (Sinopharm Chemical Reagent Beijing Co. Ltd., China) was slowly added under mechanical agitation. Afterward, 20 mL of $FeCl_2$ (0.02 M) and 40 mL of $FeCl_3$ (0.02 M) (Sinopharm Chemical Reagent Beijing Co. Ltd., China) were introduced. A black-colored precipitate was immediately formed after mechanical agitation for 10 min. The precipitate was collected by centrifugation, washed with deionized water several times, and dried at 60 °C for 6 h.

2.2. Synthesis of $BiVO_4$ and $BiVO_4/Fe_3O_4$ submicron structures

To obtain porous peanut-like $BiVO_4$ submicron structures, 2 mmol of $Bi(NO_3)_3 \cdot 5H_2O$ (Sinopharm Chemical Reagent Beijing Co. Ltd., China) was dissolved in 10 mL of ethylene glycol (Sinopharm Chemical Reagent Beijing Co., Ltd., China) under magnetic stirring for 15 min. After that, 2 mmol of NH_4VO_3 (Sinopharm Chemical Reagent Beijing Co., Ltd., China) was added into the solution under vigorous stirring followed by the addition of 10 mL of deionized water. After being well homogenized, the final yellow-colored precursor was transferred into a 30 mL Teflon-lined stainless steel autoclave, sealed and maintained at 160 °C for 24 h. The yellow-colored precipitate formed was separated by centrifugation, washed with deionized water several times and dried at 60 °C for 6 h. Porous peanut-like $BiVO_4/Fe_3O_4$ submicron structures were synthesized under the same experimental conditions with the addition of 10 wt% Fe_3O_4 nanoparticles.

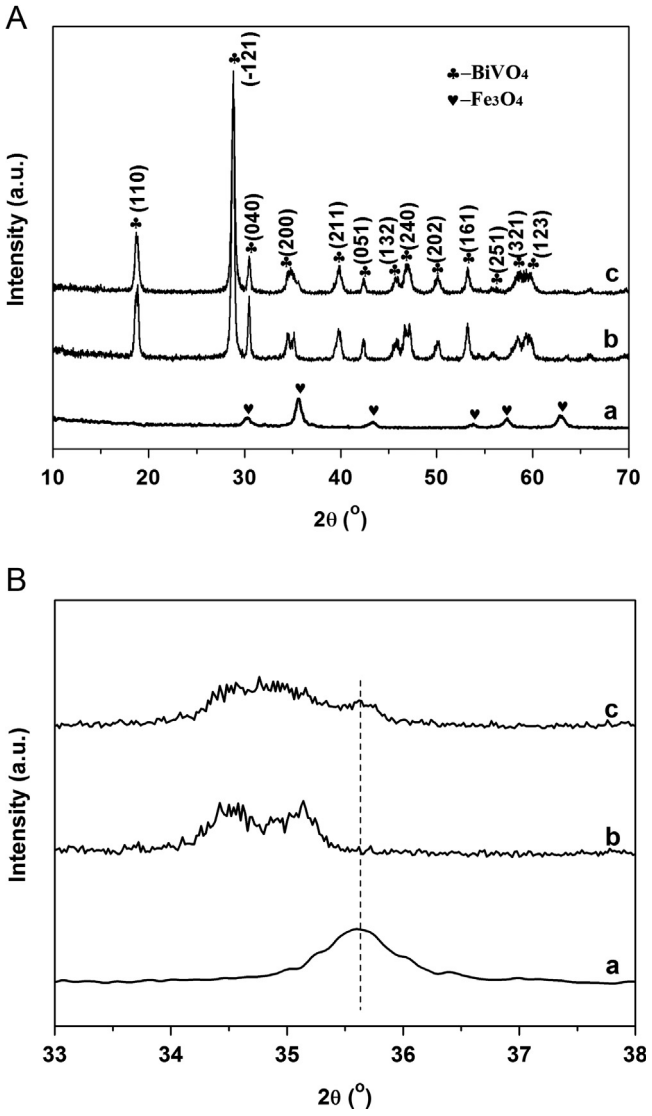

Fig. 1. XRD patterns of Fe_3O_4 (a), $BiVO_4$ (b) and $BiVO_4/Fe_3O_4$ (c) powders synthesized by chemical precipitation method at room temperature and hydrothermal method at 160 °C for 24 h, respectively (A). XRD patterns of Fe_3O_4 (a), $BiVO_4$ (b) and $BiVO_4/Fe_3O_4$ (c) powders synthesized by chemical precipitation method at room temperature and hydrothermal method at 160 °C for 24 h, respectively, in the range of $2\theta = 33-38°$ (B).

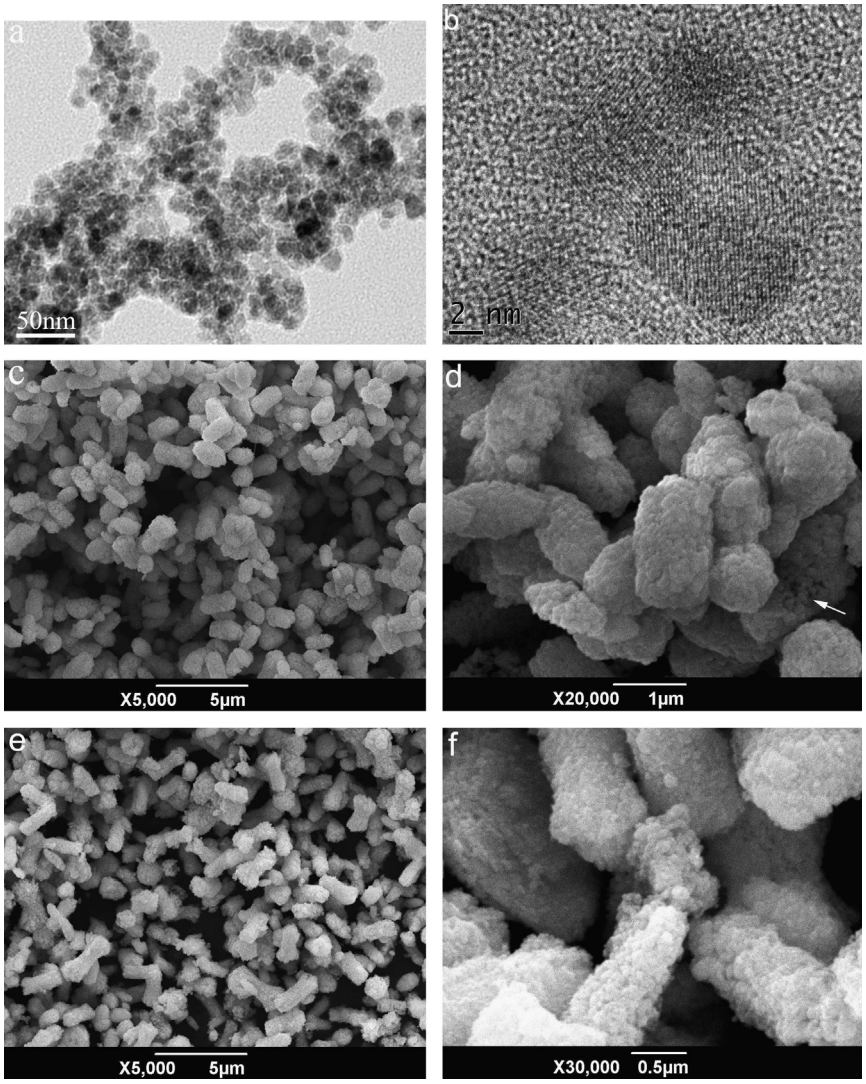

Fig. 2. TEM (a) and HRTEM (b) images of Fe_3O_4 powders synthesized by chemical precipitation method at room temperature. SEM images of $BiVO_4$ (c, d) and $BiVO_4/Fe_3O_4$ (e, f) powders synthesized by hydrothermal method at 160 °C for 24 h.

2.3. Characterization

The crystalline phases of the samples were identified by X-ray powder diffraction using a D/Max2550 X-ray diffractometer (Rigaku, Japan) with Cu Kα radiation (λ=1.5406 Å). The powder samples were scanned at a scanning rate of 5°/min in the 2θ range of 10–70° at 40 kV and 50 mA. The morphologies of the samples were observed by using a Quanta 200 scanning electron microscope (FEI, The Netherlands) equipped with energy-dispersive X-ray spectrometer (EDX). The transmission electron microscopy (TEM) and high-resolution transmission electron microscopy (HRTEM) images of the samples were taken with a JEM-2100 electron microscope (JEOL, Japan) with an acceleration voltage of 200 kV. X-ray photoelectron spectroscopy (XPS) analysis was performed on an ESCALAB MKII X-ray photoelectron spectrometer (VG Scientific, UK) using Mg Kα radiation. The UV–vis diffuse reflectance spectra were measured using a Lambda 950 UV–vis-NIR spectrophotometer (Perkin-Elmer, USA) in the wavelength range of 200–750 nm. The magnetic properties of the samples were analyzed by using a vibrating sample magnetometer (Lake Shore Cryotronics, Inc., USA) at room temperature.

2.4. Photodegradation experiments

The photodegradation of Rhodamine B (RhB) and methylene blue (MB) over the as-synthesized samples was performed under visible light irradiation using a 400 W metal halide lamp with a cutoff filter ($\lambda > 400$ nm). The reaction temperature was maintained at 25 °C by using water in the cooling jacket of the reactor. The initial concentration of RhB (or MB) was 10 mg/L and the photocatalyst used was 1.0 g/L. The suspension was first sonicated for 10 min and then stirred in the dark for 30 min to ensure adsorption/desorption equilibrium prior to visible light irradiation. During visible light irradiation, 2 mL of suspension was taken out at certain time intervals for subsequent RhB (or MB) concentration analysis. The RhB and

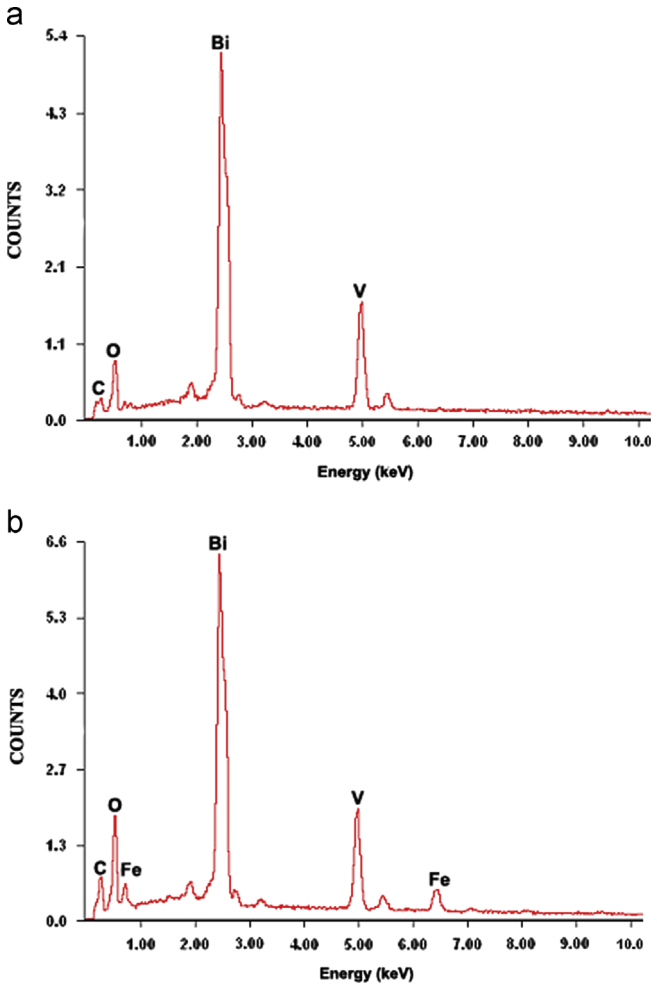

Fig. 3. EDX spectra of $BiVO_4$ (a) and $BiVO_4/Fe_3O_4$ (b) powders synthesized by hydrothermal method at 160 °C for 24 h.

MB concentrations were analyzed by using a U-3010 UV–vis spectrophotometer (Hitachi, Japan).

3. Results and discussion

Fig. 1A (a) shows the XRD pattern of the Fe_3O_4 powders synthesized by a simple chemical precipitation method at room temperature. All the diffraction peaks in the XRD pattern can be indexed to cubic Fe_3O_4 (JCPDS card no. 74-0748). No characteristic peaks corresponding to impurity phases (Fe_2O_3 and FeOOH) were observed, indicating high purity of the as-synthesized Fe_3O_4 powders. The crystallite size of the Fe_3O_4 powders estimated using Scherrer's formula is about 10 nm. The XRD patterns of the $BiVO_4$ and $BiVO_4/Fe_3O_4$ powders hydrothermally synthesized at 160 °C for 24 h are shown in Fig. 1A (b) and (c). All the diffraction peaks can be corresponded to monoclinic $BiVO_4$ (JCPDS card no.14-0688) with the space group of I2/a(15). The diffraction peaks with high intensity indicate high crystallinity of the $BiVO_4$ powders. To confirm the formation of $BiVO_4/Fe_3O_4$ composite photocatalyst, the XRD patterns shown in Fig. 1A are magnified and shown in Fig. 1B with 2θ range of 33–38°. A diffraction peak belonging to the Fe_3O_4 phase is found at $2\theta = 35.6°$ with low intensity in the XRD pattern of $BiVO_4/Fe_3O_4$ composite photocatalyst. The XRD pattern of the $BiVO_4$ powders does not have that diffraction peak.

The morphologies of the samples were observed by using scanning (SEM) and transmission (TEM) electron microscopy and the results are illustrated in Fig. 2. Fig. 2a and b show the TEM and HRTEM images of the Fe_3O_4 powders synthesized by chemical precipitation method at room temperature. Apparently, the Fe_3O_4 nanoparticles have nearly a spherical shape with the average diameter of 5–12 nm (Fig. 2a), which is

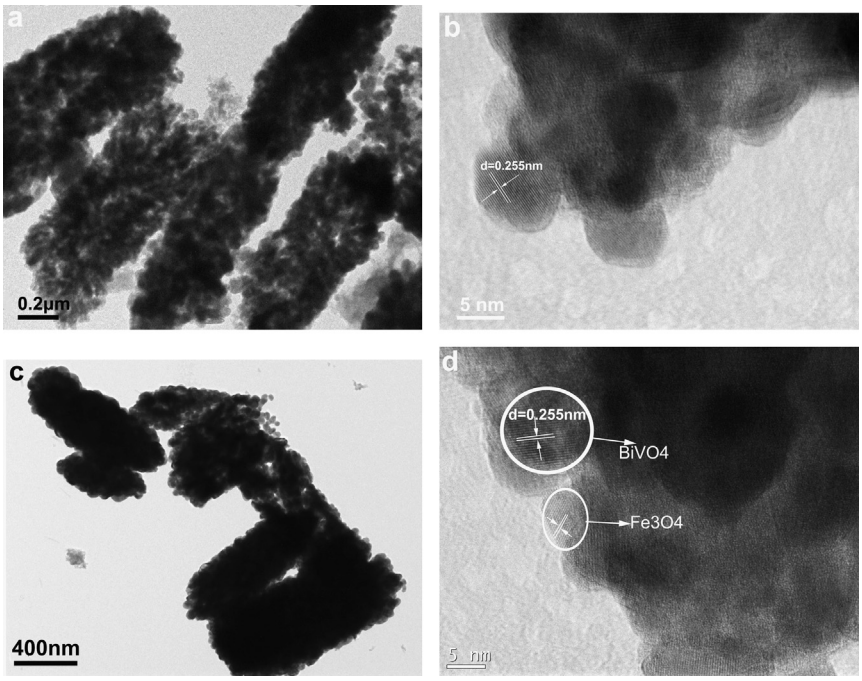

Fig. 4. TEM and HRTEM images of $BiVO_4$ (a, b) and $BiVO_4/Fe_3O_4$ (c, d) powders synthesized by hydrothermal method at 160 °C for 24 h.

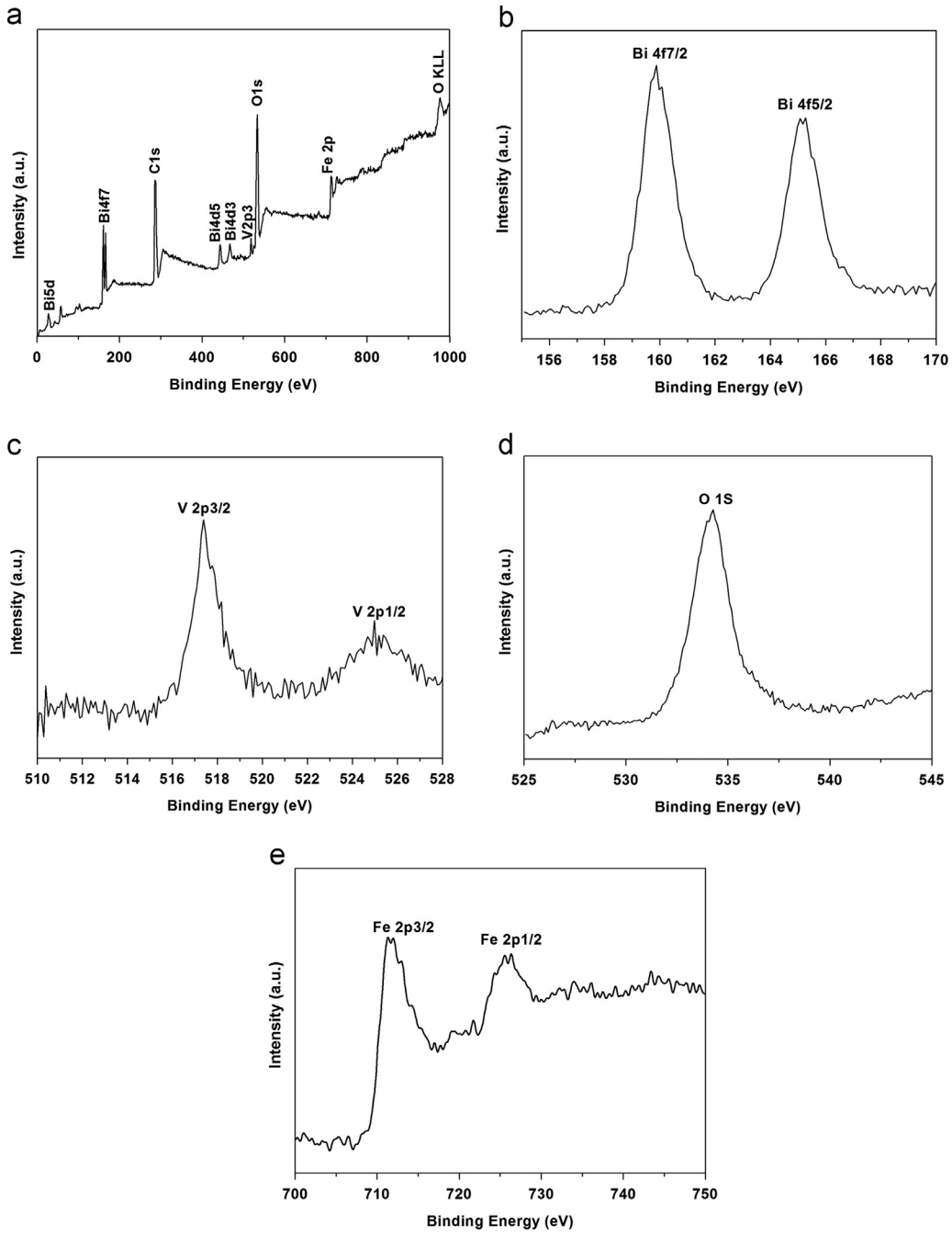

Fig. 5. XPS survey spectrum (a) and XPS spectra of Bi (b), V (c), O (d) and Fe (e) in the $BiVO_4/Fe_3O_4$ composite photocatalyst synthesized by hydrothermal method at 160 °C for 24 h.

consistent with the crystallite size of the sample estimated using the Scherrer's formula. The HRTEM image shown in Fig. 2b confirms that each Fe_3O_4 nanoparticle has a single-crystal nature. Fig. 2c represents SEM micrograph of the $BiVO_4$ powders synthesized by hydrothermal method at 160 °C for 24 h. It is visible that the $BiVO_4$ powders are composed of large-scale peanut-like structures with the lengths of 500–800 nm and the widths of 300–500 nm. A magnified SEM micrograph in Fig. 2d shows that each peanut-like submicron structure is composed of a large number of nanoparticles and has a porous structure. The SEM micrograph shown in Fig. 2e confirms that the $BiVO_4/Fe_3O_4$ composite photocatalyst has peanut-like submicron structures. Similar to $BiVO_4$, each peanut-like submicron structure of $BiVO_4/Fe_3O_4$ composite photocatalyst having a porous structure is composed of tiny nanoparticles (Fig. 2f). The elemental compositions of the $BiVO_4$ and $BiVO_4/Fe_3O_4$ powders were analyzed by an energy dispersive X-ray spectroscopy (EDX). As indicated in the EDX spectra, bismuth, vanadium and oxygen are present in $BiVO_4$ powders (Fig. 3a), whereas bismuth, vanadium, oxygen and iron are noted for $BiVO_4/Fe_3O_4$ composite photocatalyst (Fig. 3b).

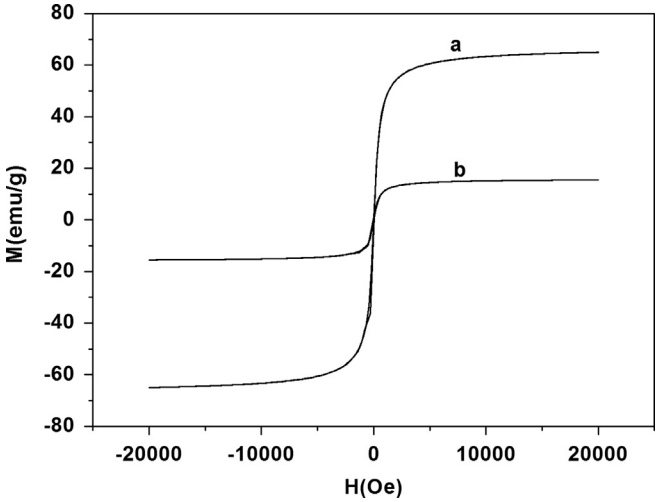

Fig. 6. *M–H* curves of Fe_3O_4 (a) and $BiVO_4/Fe_3O_4$ (b) powders synthesized by chemical precipitation method at room temperature and hydrothermal method at 160 °C for 24 h, respectively.

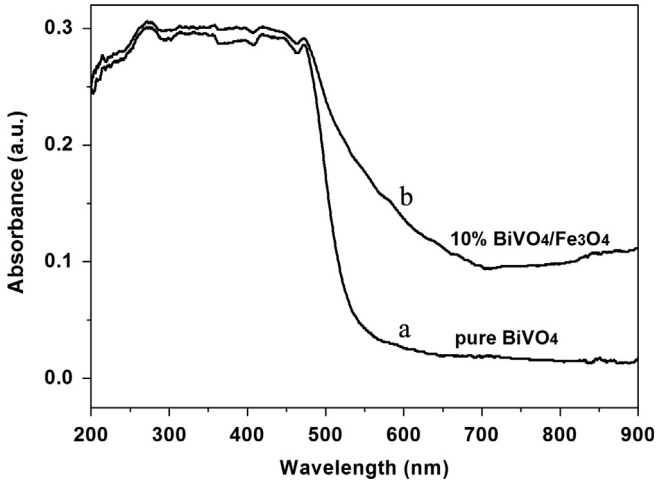

Fig. 7. UV–vis diffuse reflectance spectra of $BiVO_4$ (a) and $BiVO_4/Fe_3O_4$ (b) powders synthesized by hydrothermal method at 160 °C for 24 h.

To further investigate the crystal structures of $BiVO_4$ and $BiVO_4/Fe_3O_4$ powders, the samples were observed by TEM. Fig. 4 shows the TEM and HRTEM images of the $BiVO_4$ and $BiVO_4/Fe_3O_4$ powders synthesized by hydrothermal method at 160 °C for 24 h. Fig. 4a shows the TEM image of $BiVO_4$ powders, evidencing that the self-assembly of nanoparticles with size of about 5–10 nm led to the formation of porous peanut-like $BiVO_4$ submicron structures. The HRTEM image in Fig. 4b indicates that the $BiVO_4$ nanoparticles formed have a single-crystal nature. The lattice fringes of 0.255 nm observed on single crystallite agree with the (001) lattice plane of $BiVO_4$. Fig. 4c shows the TEM image of the $BiVO_4/Fe_3O_4$ submicron structures. As can be seen, peanut-like submicron structures with porous structure are composed of nanoparticles. The HRTEM image in Fig. 4d indicates two different lattice fringes of 0.255 nm and 0.240 nm observed on composite photocatalyst which are consistent with the (0 0 1) lattice plane of $BiVO_4$ and (311) lattice plane of Fe_3O_4, respectively.

To elucidate the elemental compositions and chemical states of Bi, V and Fe in $BiVO_4/Fe_3O_4$ composite photocatalyst, X-ray photoelectron spectroscopy (XPS) analysis was performed. The binding energy of 284.6 eV for C (1s) was used as a reference. Fig. 5a shows XPS survey spectrum of $BiVO_4/Fe_3O_4$ composite photocatalyst that clearly shows the binding energies for Bi (4s), Bi (4f), Bi (4d), Bi (5d), Fe (2p), V (2p), O (1s), and C (1s). Fig. 5b–e shows XPS spectra of Bi (b), V (c), O (d) and Fe (e) in $BiVO_4/Fe_3O_4$ composite photocatalyst. As shown in Fig. 5b and d, the binding energies of Bi $4f_{7/2}$, Bi $4f_{5/2}$ and O 1s are 159.0, 164.0 and 528.0 eV, respectively. The V 2p orbital has two binding energies of 525.0 eV and 517 eV for V $2p_{1/2}$ and V $2p_{3/2}$, respectively (Fig. 5d). Fig. 5e shows two bands with binding energies of 710.3 eV and 723.9 eV that can be assigned to Fe $2p_{3/2}$ and Fe $2p_{1/2}$, respectively. Both bands are consisted of Fe^{2+} (FeO) and Fe^{3+} (Fe_2O_3) peaks and are typical characteristics of Fe_3O_4 [27,32]. The obtained results confirm the formation of $BiVO_4/Fe_3O_4$ composite photocatalyst.

The magnetic properties of Fe_3O_4 and $BiVO_4/Fe_3O_4$ powders were analyzed using a vibrating sample magnetometer (VSM) at room temperature. As shown in Fig. 6, the coercivity of both samples is almost negligible at 300 K, indicating that Fe_3O_4 and $BiVO_4/Fe_3O_4$ powders are superparamagnetic at room temperature. The saturation magnetization of Fe_3O_4 nanoparticles is about 64 emu g^{-1} (curve a), whereas the saturation magnetization of $BiVO_4/Fe_3O_4$ composite photocatalyst is about 15 emu g^{-1} (curve b). Strong magnetization of $BiVO_4/Fe_3O_4$ composite photocatalyst indicates that it can be easily separated from solution after photodegradation experiment by applying an external magnetic field.

Fig. 7 shows the UV–vis diffuse reflectance spectra of $BiVO_4$ and $BiVO_4/Fe_3O_4$ powders. As can be noted, both samples have strong visible light absorption. By comparing these UV–vis diffuse reflectance spectra, a red shift is observed for the $BiVO_4/Fe_3O_4$ composite photocatalyst. This might be resulted from the presence of Fe_3O_4 nanoparticles in the $BiVO_4/Fe_3O_4$ composite photocatalyst. According to the results shown, the $BiVO_4/Fe_3O_4$ composite photocatalyst has become effective for the degradation of organic pollutants under visible light irradiation.

The photocatalytic activity of Fe_3O_4, $BiVO_4$ and $BiVO_4/Fe_3O_4$ powders was evaluated by the degradation of RhB under visible light irradiation ($\lambda > 400$ nm) at room temperature. The temporal changes in the concentration of RhB were monitored by examining the variation in maximal absorption of UV–vis spectra at 554 nm. Fig. 8a shows photocatalytic performance (C/C_0) of Fe_3O_4, $BiVO_4$ and $BiVO_4/Fe_3O_4$ powders for the degradation of RhB with and without the assistance of H_2O_2 versus visible light irradiation time. For comparison purposes, we additionally performed experiments for direct photolysis of RhB (blank experiment) without photocatalyst under the same experimental conditions with 0.1 mL of H_2O_2. Apparently, a blank experiment in the absence of photocatalyst showed no obvious change in RhB concentration within 100 min under visible light irradiation. The photodegradation of RhB over Fe_3O_4 and $BiVO_4$ powders under visible light

irradiation is low, that is, about 16% and 40% in 100 min, respectively. Interestingly, $BiVO_4$ showed relatively low photocatalytic activity for the degradation of RhB although it has strong visible light absorbance (Fig. 7). Hence, the photocatalytic activity of $BiVO_4$ could be improved with the incorporation of Fe_3O_4. The total photodegradation of RhB over $BiVO_4/Fe_3O_4$ composite photocatalyst was about 60%. The reason is that the migration of electron–hole pairs in $BiVO_4$ catalyst is limited. So, the photodegradation of RhB over $BiVO_4$ powders needs relatively longer irradiation time. Similar results were previously reported for $BiVO_4$ powders [15,16]. After the incorporation of Fe_3O_4 nanoparticles, the $BiVO_4/Fe_3O_4$ composite photocatalyst became more effective in absorbing visible light (Fig. 7), leading to enhanced photocatalytic activity for the degradation of organic dyes under visible light irradiation. Furthermore, coupling narrow-band-gap semiconductors with wide-band-gap semiconductors not only enhances optical absorption ability but also facilitates the separation of the photogenerated carriers under internal field induced by the different electronic band structures [33,34]. Therefore, the composite photocatalyst containing $BiVO_4$ (E_g=2.4 eV) and Fe_3O_4 (E_g=0.1 eV) shows higher photocatalytic activity than single ones under visible light irradiation. It is worth to note that the photocatalytic activity of Fe_3O_4, $BiVO_4$ and $BiVO_4/Fe_3O_4$ powders was significantly improved by introducing H_2O_2 into the RhB aqueous solution. The total photodegradation of RhB over Fe_3O_4, $BiVO_4$ and $BiVO_4/Fe_3O_4$ powders was up to 50%, 85% and 99%, respectively, with the assistance of H_2O_2. The UV–vis spectra of RhB solution after different visible light irradiation times over $BiVO_4/Fe_3O_4$ photocatalyst composite with the assistance of H_2O_2 are plotted in Fig. 8b. It is clear that the absorption peak at 554 nm decreases dramatically as visible light irradiation time increases and nearly disappears within 100 min.

Methylene blue (MB) was also chosen to investigate the photocatalytic activity of Fe_3O_4, $BiVO_4$ and $BiVO_4/Fe_3O_4$ composite photocatalyst. Fig. 8c shows photocatalytic performance (C/C_0) of Fe_3O_4, $BiVO_4$ and $BiVO_4/Fe_3O_4$ powders for the degradation of MB with and without the assistance of H_2O_2 versus visible light irradiation time. For comparison purposes, we additionally performed experiments for direct photolysis of MB (blank experiment) without photocatalyst under the same experimental conditions with 0.1 mL of H_2O_2. Apparently, blank experiments with and without the assistance of H_2O_2 showed negligible changes in MB concentration (5.1% and 9.2%) within 140 min under visible light irradiation. The $BiVO_4/Fe_3O_4$ composite photocatalyst shows good photocatalytic activity than Fe_3O_4 and $BiVO_4$ for the photodegradation of MB. The total photodegradation of MB over $BiVO_4/Fe_3O_4$ sample without the assistance of H_2O_2 in the reaction solution was 75% under visible light irradiation for 120 min. Nevertheless, the photocatalytic activity of Fe_3O_4, $BiVO_4$ and

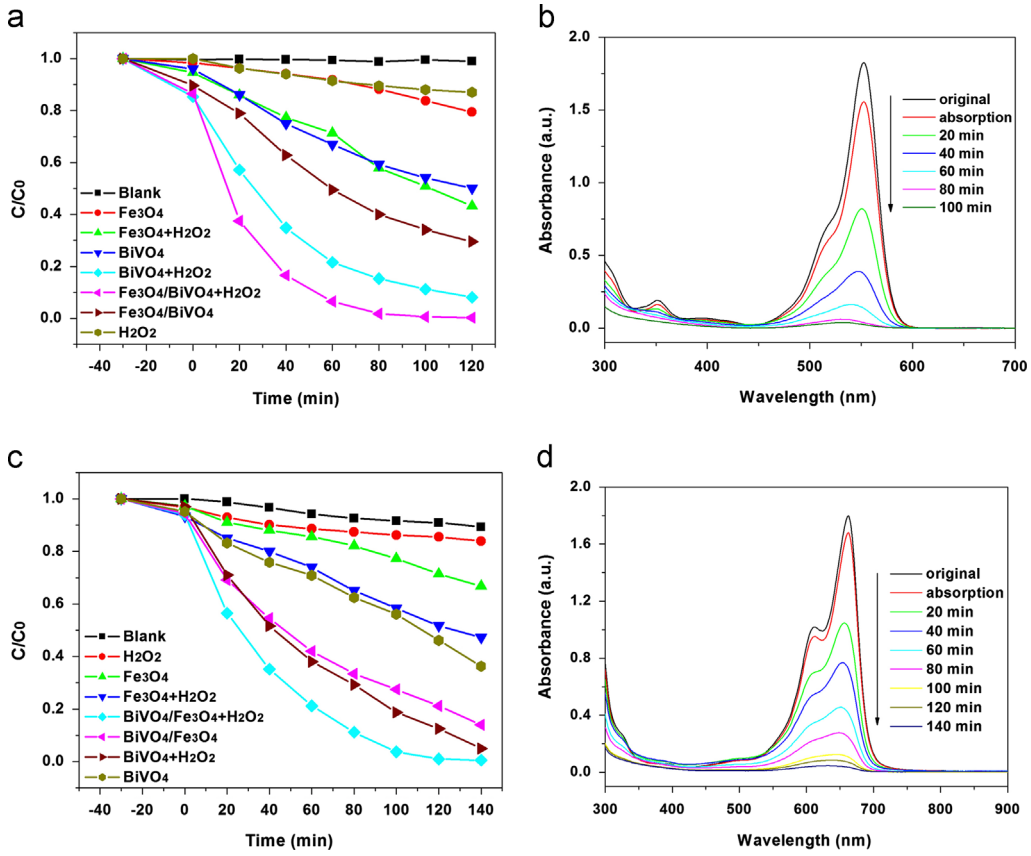

Fig. 8. The photocatalytic performance (C/C_0) of Fe_3O_4, $BiVO_4$ and $BiVO_4/Fe_3O_4$ for the degradation of RhB and MB with and without H_2O_2 versus visible light irradiation time (a, c). The temporal evolution of the spectra of RhB and MB solutions in the presence of $BiVO_4/Fe_3O_4$ composite photocatalysts under visible light irradiation with the addition of H_2O_2 (b, d).

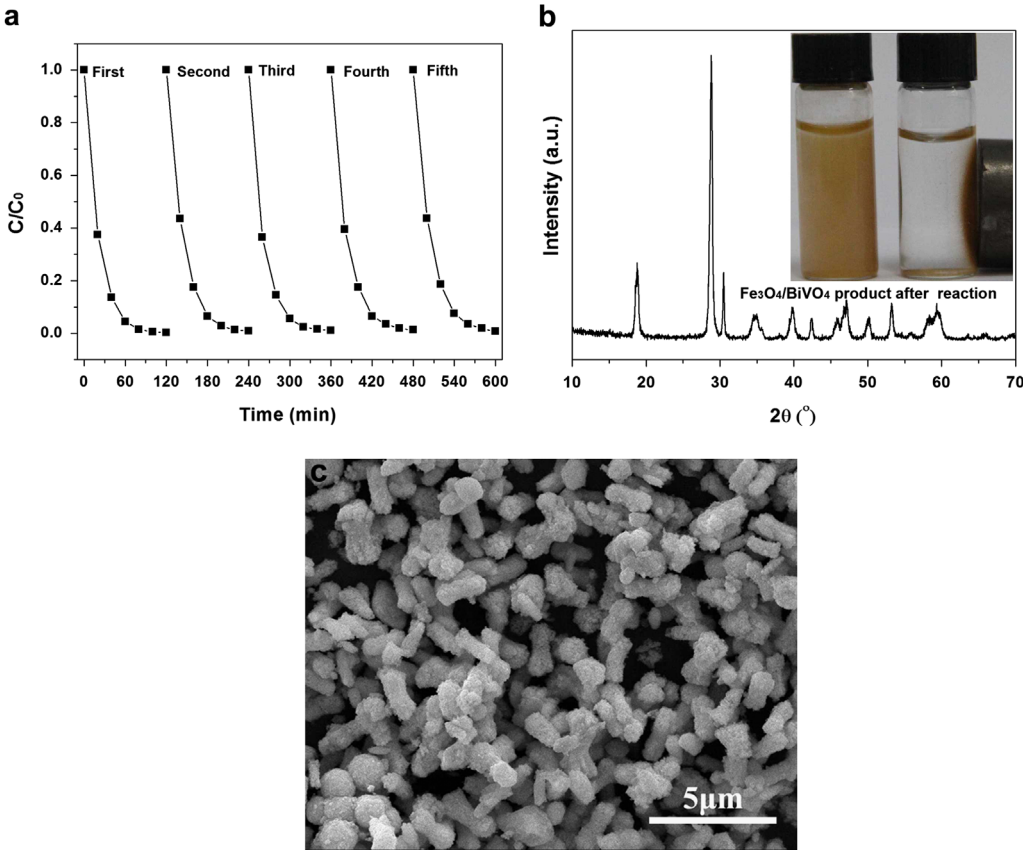

Fig. 9. Recycling test on the $BiVO_4/Fe_3O_4$ composite photocatalyst for the degradation of RhB under visible light irradiation (a). The initial RhB concentration was 10 mg/L, the $BiVO_4/Fe_3O_4$ composite photocatalyst was 1.0 g/L, and the volume of H_2O_2 introduced for each run was 0.1 mL. XRD pattern (b) and SEM image (c) of $BiVO_4/Fe_3O_4$ composite photocatalyst after five cycles of photodegradation experiments.

$BiVO_4/Fe_3O_4$ composite photocatalyst was considerably improved by introducing H_2O_2 into the MB aqueous solution. The total photodegradation of MB over Fe_3O_4, $BiVO_4$ and $BiVO_4/Fe_3O_4$ powders reached 50%, 86% and 98%, respectively, in the presence of H_2O_2 under visible light irradiation for 120 min. The UV–vis spectra of MB solution after different visible light irradiation times over $BiVO_4/Fe_3O_4$ photocatalyst composite with the assistance of H_2O_2 are plotted in Fig. 8d. It is clear that the absorption peak at 653 nm decreases dramatically as visible light irradiation time increases and nearly disappears within 120 min.

H_2O_2 is widely used in photocatalytic processes of wastewater treatment. As an environmentally benign oxidant, H_2O_2 can provide hydroxyl radicals (•OH) to advanced oxidation processes, such as O_3/H_2O_2, UV/H_2O_2, and photo-Fenton processes [34–37]. In recent years, several studies have shown that H_2O_2 can enhance the photodegradation of organic dyes under visible light irradiation [37–40]. Therefore, the following possible photocatalytic reactions may take place in the $Fe_3O_4/BiVO_4/H_2O_2$ system under visible light irradiation:

$$BiVO_4 + h\nu \rightarrow h^+ + e^- \quad (1)$$

$$Fe_3O_4 + h\nu \rightarrow h^+ + e^- \quad (2)$$

$$H_2O_2 + e^- \rightarrow HO^\bullet + OH^- \quad (3)$$

$$\text{RhB (or MB)} + HO^\bullet \rightarrow \text{degradation products} \quad (4)$$

$$\text{RhB (or MB)} + h^+ \rightarrow \text{degradation products} \quad (5)$$

To study the photostability of $BiVO_4/Fe_3O_4$ composite photocatalyst during photocatalytic reactions under visible light irradiation, the sample was collected, dried and reused in five successive photocatalytic experiments. Fig. 9a shows the results of five successive runs for the photodegradation of RhB over $BiVO_4/Fe_3O_4$ composite photocatalyst under the same experimental conditions: pH, initial RhB concentration and ionic strength. As can be seen in Fig. 9a, the $BiVO_4/Fe_3O_4$ composite photocatalyst retains its high photocatalytic activity ($>98\%$) in five successive runs, each of which lasted for 80 min. More importantly, the crystal structure (Fig. 9b) and morphology (Fig. 9c) of $BiVO_4/Fe_3O_4$ composite photocatalyst remained unchanged even after five successive runs, indicating high stability of composite photocatalyst under visible light irradiation. We believe that the magnetic property of $BiVO_4/Fe_3O_4$ composite photocatalyst was essential for efficient recycling of the composite photocatalyst in liquid-phase reactions. As an example, shown in the inset of Fig. 9b, when the $BiVO_4/Fe_3O_4$ composite photocatalyst was dispersed in water, the suspension turned into a black color. By applying an external magnetic field, the black particles suspended in the solution were readily harvested within 30 s and the solution became transparent.

4. Conclusions

Porous peanut-like $BiVO_4$ and $BiVO_4/Fe_3O_4$ composite photocatalyst with submicron structures were synthesized by a template-free hydrothermal method and their photocatalytic activity was evaluated for the degradation of RhB and MB under visible light irradiation with and without H_2O_2. The obtained results demonstrated that porous peanut-like $BiVO_4/Fe_3O_4$ composite photocatalyst showed higher photocatalytic activity in the H_2O_2-assisted system under visible light irradiation compared to $BiVO_4$. Recycling test on the $BiVO_4/Fe_3O_4$ composite photocatalyst for the degradation of RhB under visible light irradiation showed that the composite photocatalyst was stable in the H_2O_2-assisted system in five cycles. Therefore, this composite photocatalyst will be beneficial for the degradation of organic pollutants present in water and air under solar light.

Acknowledgments

This work was supported by the National Natural Science Foundation of China (Program nos. 51102160 and 51272148) and the Fundamental Research Funds for the Central Universities (Program no. GK201102027). MH would like to thank the Japan Society for the Promotion of Science (JSPS) for the financial support.

References

[1] A. Fujishima, K. Honada, Electrochemical photolysis of water at a semiconductor electrode, Nature 238 (1972) 37–38.
[2] M. Inagaki, N. Kondo, R. Nonaka, E. Ito, M. Toyoda, K. Sogabe, T. Tsumura, Structure and photoactivity of titania derived from nanotubes and nanofibers, Journal of Hazardous Materials 161 (2009) 1514–1521.
[3] Z. Zhou, J. Ye, K. Sayama, H. Arakawa, Direct splitting of water under visible light irradiation with an oxide semiconductor photocatalyst, Nature 414 (2001) 625–627.
[4] Z. Bian, J. Zhu, S. Wang, Y. Cao, X. Qian, H. Li, Self-assembly of active Bi_2O_3/TiO_2 visible photocatalyst with ordered mesoporous structure and highly crystallized anatase, Journal of Physical Chemistry C 112 (2008) 6258–6262.
[5] W.I.F. David, I.G. Wood, Ferroelastic phase transition in BiVO4: VI. Some comments on the relationship between spontaneous deformation and domain walls in ferroelastics, Journal of Physics C: Solid State Physics, 16, 5149–5166.
[6] K. Hirota, G. Komatsu, M. Yamashita, H. Takemura, O. Yamaguchi, Formation, characterization and sintering of alkoxy-derived bismuth vanadate, Materials Research Bulletin 27 (1992) 823–830.
[7] K. Shantha, K.B.R. Varma, Preparation and characterization of nanocrystalline powders of bismuth vanadate, Materials Science and Engineering B 60 (1999) 66–75.
[8] A. Galembeck, O.L. Alves, $BiVO_4$ thin film preparation by metalorganic decomposition, Thin Solid Films 365 (2000) 90–93.
[9] T. Yang, D. Xia, Self-assembly of highly crystalline spherical $BiVO_4$ in aqueous solutions, Journal of Crystal Growth 311 (2009) 4505–4509.
[10] H.M. Zhang, J.B. Liu, H. Wang, W.X. Zhang, H. Yan, Rapid microwave-assisted synthesis of phase controlled $BiVO_4$ nanocrystals and research on photocatalytic properties under visible light irradiation, Journal of Nanoparticle Research 10 (2008) 767–774.
[11] X. Zhang, Y. Zhang, X. Quan, S. Chen, Preparation of Ag doped $BiVO_4$ film and its enhanced photoelectrocatalytic (PEC) ability of phenol degradation under visible light, Journal of Hazardous Materials 167 (2009) 911–914.
[12] M. Shang, W. Wang, L. Zhou, S. Sun, W. Yin, Nanosized $BiVO_4$ with high visible-light-induced photocatalytic activity: Ultrasonic-assisted synthesis and protective effect of surfactant, Journal of Hazardous Materials 172 (2009) 338–344.
[13] S. Tokunaga, H. Kato, A. Kudo, Selective preparation of monoclinic and tetragonal $BiVO_4$ with scheelite structure and their photocatalytic properties, Chemistry of Materials 13 (2001) 4624–4628.
[14] T.L. Thompson, J.T. Yates Jr., Surface science studies of the photoactivation of TiO_2-new photochemical processes, Chemical Reviews 106 (2006) 4428–4453.
[15] A. Zhang, J. Zhang, N. Cui, X. Tie, Y. An, L. Li, Effects of pH on hydrothermal synthesis and characterization of visible-light-driven $BiVO_4$ photocatalyst, Journal of Molecular Catalysis A 304 (2009) 28–32.
[16] X. Zhang, Z. Ai, F. Jia, L. Zhang, X. Fan, Z. Zou, Selective synthesis and visible-light photocatalytic activities of $BiVO_4$ with different crystalline phases, Materials Chemistry and Physics 103 (2007) 162–167.
[17] H.Q. Jiang, H. Endo, H. Natori, M. Nagai, K. Kobayashi, Fabrication and photoactivities of spherical-shaped $BiVO_4$ photocatalysts through solution combustion synthesis method, Journal of the European Ceramic Society 28 (2008) 2955–2962.
[18] G. Xi, J. Ye, Synthesis of bismuth vanadate nanoplates with exposed {001} facets and enhanced visible-light photocatalytic properties, Chemical Communications 46 (2010) 1893–1895.
[19] L. Zhang, D. Chen, X. Jiao, Monoclinic structured $BiVO_4$ nanosheets: hydrothermal preparation, formation mechanism, and coloristic and photocatalytic properties, Journal of Physical Chemistry B 110 (2006) 2668–2673.
[20] Y. Sun, Y. Xie, C. Wu, S. Zhang, S. Jiang, Aqueous synthesis of mesostructured $BiVO_4$ quantum tubes with excellent dual response to visible light and temperature, Nano Research 3 (2010) 620–631.
[21] L. Ren, L. Ma, L. Jin, J. Wang, M. Qiu, Y. Yu, Template-free synthesis of $BiVO_4$ nanostructures: II. Relationship between various microstructures for monoclinic $BiVO_4$ and their photocatalytic activity for the degradation of Rhodamine B under visible light, Nanotechnology, 20, 405602–405609.
[22] G. Li, D. Zhang, J. Yu, Ordered mesoporous $BiVO_4$ through nanocasting: a superior visible light-driven photocatalyst, Chemistry of Materials 20 (2008) 3983–3992.
[23] M. Shang, W. Wang, J. Ren, S. Sun, L. Zhang, A novel $BiVO_4$ hierarchical nanosturcture: controllable synthesis, growth mechanism, and application in photocatalysis, Crystal Engineering Communications 12 (2010) 1754–1758.
[24] H. Gu, K. Xu, C. Xu, B. Xu, Biofunctional magnetic nanoparticles for protein separation and pathogen detection, Chemical Communications (2006) 941–949.
[25] K. Cheng, S. Peng, C. Xu, S. Sun, Porous hollow Fe_3O_4 nanoparticles for targeted delivery and controlled release of cisplatin, Journal of American Chemical Society 131 (2009) 10637–10644.
[26] S. Laurent, D. Forge, M. Port, A. Roch, C. Robic, L.V. Elst, R.N. Muller, Magnetic iron oxide nanoparticles: synthesis, stabilization, vectorization, physicochemical characterizations, and biological applications, Chemical Reviews 108 (2008) 2064–2100.
[27] S. Xuan, W. Jiang, X. Gong, Y. Hu, Z. Chen, Magnetically separable Fe_3O_4/TiO_2 hollow spheres: fabrication and photocatalytic activity, Journal of Physical Chemistry C 113 (2009) 553–558.
[28] Y. Liu, L. Zhou, Y. Hu, C. Guo, H. Qian, F. Zhang, X.W. Lou, Magnetic-field induced formation of 1D Fe_3O_4/C/CdS coaxial nanochains as highly efficient and reusable photocatalysts for water treatment, Journal of Materials Chemistry 21 (2011) 18359–18364.
[29] Y. Wang, S. Li, X. Xing, F. Huang, Y. Shen, A. Xie, X. Wang, J. Zhang, Self-assembled 3D flowerlike hierarchical $Fe_3O_4@Bi_2O_3$ core–shell architectures and their enhanced photocatalytic activity under visible light, Chemistry—A European Journal 17 (2011) 4802–4808.
[30] G. Xi, B. Yue, J. Cao, J. Ye, Fe_3O_4/WO_3 hierarchical core–shell structure: high-performance and recyclable visible-light photocatalysis, Chemistry—A European Journal 17 (2011) 5145–5154.
[31] S.K. Li, F.Z. Huang, Y. Wang, Y.H. Shen, L.G. Qiu, A.J. Xie, S.J. Xu, Magnetic $Fe_3O_4@C@Cu_2O$ composites with bean-like core/shell nanostructures: synthesis, properties and application in recyclable photocatalytic degradation of dye pollutants, Journal of Materials Chemistry 21 (2011) 7459–7466.

[32] C.L. Zhu, M.L. Zhang, Y.J. Qiao, G. Xiao, F. Zhang, Y.J. Chen, Fe_3O_4/TiO_2 core/shell nanotubes: synthesis and magnetic and electromagnetic wave absorption characteristics, Journal of Physical Chemistry C 114 (2010) 16229–16235.
[33] J. Zhang, Q. Xu, Z.C. Feng, C. Li, Importance of the relationship between surface phases and photocatalytic activity of TiO_2, Angewandte Chemie International Edition 47 (2008) 1766–1769.
[34] F.L. Zhang, W.Z. Wang, L. Zhou, M. Shang, S.M. Sun, Fe_3O_4 coupled BiOCl: a highly efficient magnetic photocatalyst, Applied Catalysis B 90 (2009) 458–462.
[35] F. Javier Benitez, F.J. Real, J.L. Acero, C. Garcia, Photochemical oxidation processes for the elimination of phenyl–urea herbicides in waters, Journal of Hazardous Materials 138 (2006) 278–287.
[36] J. Ma, W. Ma, W. Song, C. Chen, Y. Tang, J. Zhao, Y. Huang, Y. Xu, L. Zang, Fenton degradation of organic pollutants in the presence of low-molecular-weight organic acids: Cooperative effect of quinone and visible light, Environmental Science and Technology 40 (2006) 618–624.
[37] S. Kaniou, K. Pitarakis, I. Barlagianni, I. Poulios, Photocatalytic oxidation of sulfamethazine, Chemosphere 60 (2005) 372–380.
[38] L.L. Ju, Z.Y. Chen, L. Fang, W. Dong, F.G. Zheng, M.R. Shen, Sol–gel synthesis and photo-Fenton-like catalytic activity of $EuFeO_3$ nanoparticles, Journal of American Ceramic Society 94 (2011) 3418–3424.
[39] P. Lei, C. Chen, J. Yang, W. Ma, J. Zhao, L. Zang, Degradation of dye pollutants by immobilized polyoxometalate with H_2O_2 under visible-light irradiation, Environmental Science and Technology 39 (2005) 8466–8874.
[40] L. Guo, F. Chen, X. Fan, W. Cai, J. Zhang, S-doped α-Fe_2O_3 as a highly active heterogeneous Fenton-like catalyst towards the degradation of acid Orange 7 and phenol, Applied Catalysis B 96 (2010) 162–168.